(12)

207500-8-T
Final Report

CENTERLINE WAKE MODELING

M.A. True
D.R. Lyzenga
J.D. Lyden

September 1993

"Original contains color plates: All DTIC reproductions will be in black and white"

Office of Naval Research
800 N. Quincy St.
Arlington, VA 2217-5660

Contract No. N00014-90-C-0071

ERIM P.O. Box 134001
Ann Arbor, MI 48113-4001

REPORT DOCUMENTATION PAGE

Form Approved
OMB No. 0704-0188

1. AGENCY USE ONLY (Leave blank)	2. REPORT DATE	3. REPORT TYPE AND DATES COVERED
	September 1993	Final, Oct. 1992-April, 1993

4. TITLE AND SUBTITLE
Centerline Wake Modeling

5. FUNDING NUMBERS
N00014-90-C-0071

6. AUTHOR(S)
M.A. True, D.L. Lyzenga, and J.D. Lyden

7. PERFORMING ORGANIZATION NAME(S) AND ADDRESS(ES)
Environmental Research Institute of Michigan
P.O. Box 134001
Ann Arbor, MI 48113-4001

8. PERFORMING ORGANIZATION REPORT NUMBER
207500-8-T

9. SPONSORING/MONITORING AGENCY NAME(S) AND ADDRESS(ES)
Office of Naval Research
800 N. Quincy St.
Arlington, VA 2217-5660

10. SPONSORING/MONITORING AGENCY REPORT NUMBER

11. SUPPLEMENTARY NOTES

12a. DISTRIBUTION/AVAILABILITY STATEMENT
Approved for public release,
distribution is unlimited

12b. DISTRIBUTION CODE

13. ABSTRACT (Maximum 200 words)

The ERIM Ocean Model (EOM) model was used as part of an end-to-end simulation of the centerline shipwake. EOM was modified to include Milgram's turbulent damping formulation with Snyder's growth rate and Lyzenga's source-and-sink description. The EOM simulations showed that turbulent dissipation can explain the large negative modulation observed in the centerline wake. Tests were also performed to assess the sensitivity of the centerline RCS to: track aspect, incidence angle, wind direction, wind speed, surface current, and turbulence. It was found that the centerline wake width depended most strongly on the width of the turbulent dissipation region. The modulation depth was most sensitive to the turbulent damping, wind speed, and wind direction. Finally, 16 2D images of the radar cross section of the centerline shipwake were produced by EOM for use as matched filters on the experimental data.

14. SUBJECT TERMS	15. NUMBER OF PAGES
Shipwake, Synthetic Aperture Radar, Turbulence	57
	16. PRICE CODE

17. SECURITY CLASSIFICATION OF REPORT	18. SECURITY CLASSIFICATION OF THIS PAGE	19. SECURITY CLASSIFICATION OF ABSTRACT	20. LIMITATION OF ABSTRACT
Unlimited	Unlimited	Unlimited	Unlimited

CONTENTS

LIST OF FIGURES

LIST OF TABLES

1.0 INTRODUCTION AND EXECUTIVE SUMMARY

Synthetic Aperture Radar (SAR) imagery of moving ships often exhibits two distinct features:

1) The Kelvin wake composed of the gravity waves produced by the ship's passage, and
2) The centerline wake which typically manifests itself as a dark stem extending behind the ship.

These two features can be used for ship identification in the following ways. For Kelvin wakes, the wake structure can be used to identify the ship type and speed. However, the Kelvin wake is often faint or not visible in SAR images. On the other hand, the centerline shipwake is almost always observed by SAR. Whether it can be used to determine ship type and speed is yet to be determined. As a first step to that determination, an end-to-end simulation of the centerline shipwake was performed. The results were used to generate matched filters which were compared to experimental data in order to determine the validity of the end-to-end simulation.

Modeling of centerline shipwakes has been a challenging problem for some time. Simple wave-current interaction theory predicts that a sinusoidal surface current (such as the cross-track current pattern in the shipwake) produces a sinusoidal amplitude modulation. However, the dominant dark modulation apparent in centerline wake SAR images does not agree with the simple linear theory. The dark 'scar' appears to indicate more damping of the radar-reflecting Bragg waves than is predicted by interactions with the mean surface current. One possible explanation of the increased damping is turbulent dissipation.

The ERIM Ocean Model (EOM) did not include a turbulence model before the centerline shipwake project started. A turbulence model was added to EOM to test the hypothesis that it explains the dark 'scar'. Briefly, the turbulence was assumed to be a local dissipation mechanism. The functional form used in this study is due to Milgram (1991) who showed that it compared well with laboratory data and that the dissipation is wavelength dependent. Having satisfied ourselves that the wavenumber and dissipation dependence of the model was reasonable, it was incorporated into EOM.

EOM describes an important part of the shipwake physics—namely, the ocean surface dynamics and the SAR image formation—but it is not an end-to-end shipwake simulator. The shipwake simulation capability is spread throughout the ocean hydrodynamics and SAR processing community. The models required for an end-to-end shipwake simulation include: ship hydrodynamics, ocean surface dynamics, SAR image formation, and detection analysis. The organizations which have developed these programs include: DTI, SAIC, XonTech, and ERIM (among others). Their separate simulation programs have never been interfaced and run in sequence for shipwake studies. A significant task of this project was to organize and interface the inputs and outputs of the separate simulation programs.

A brief summary of the production sequence follows. First, the initial plane data for the FF, FFG, and DDG ship types were extracted from towing tank measurements and input into SAIC's FASTWAKE program. Its 2-D surface current and dissipation files were input into EOM (and SARSIM) along with the environmental conditions. The simulated SAR images from both of these programs were delivered to XonTech for matched filter analysis with the shipwake imagery supplied by Arete. The conclusion of the end-to-end simulation validation effort was that the simulated shipwakes were systematically narrower than the data.

In addition to delivering the SAR images to XonTech, a series of 2-D falsecolor images of the EOM-simulated centerline wakes were produced. Also, a series of 1-D EOM runs with only one parameter variation—a sensitivity study—augmented the experimental cases where more than one parameter varied between cases. These 1-D and 2-D simulations led to the following conclusions about the EOM portion of the end-to-end simulation:

1) The turbulence lowers the RCS of the centerline shipwake in qualitative agreement with the data.

2) The width of the centerline wake 'scar' depends primarily on the width of the turbulent dissipation region. There is also an increase in the wake width due to SAR smearing for range traveling cases.

3) The high spatial frequency of the centerline wake depends on the surface current profile.

The results of this analysis showed that a single SAR frequency and validation metric are not sufficient to validate the end-to-end simulation. The recommendations for future centerline shipwake study are directed toward a more comprehensive validation metric and observation set. In particular, 1) X band simulations and more SAR aspect cases (between range traveling and azimuth traveling) should be run, and 2) validation metrics for fine scale spatial structure should be included in the analysis.

The rest of the report is organized as follows. In Section 2, the turbulence modifications to EOM are described. In Section 3, the EOM centerline shipwake simulations are discussed. Specifically, the input data, production scenario, and SAR output images are presented. Finally, the conclusions of the centerline wake modeling are presented in Section 4.

2.0 MODIFICATION OF ERIM OCEAN MODEL TO INCLUDE TURBULENCE

2.1. REVIEW OF ERIM OCEAN MODEL

The ERIM Ocean Model (EOM) is a comprehensive set of computer programs which produce simulated SAR imagery of ocean features (Lyzenga and Bennett, 1988). The flowchart in Figure 1 shows the input, output, and processing structure of EOM.

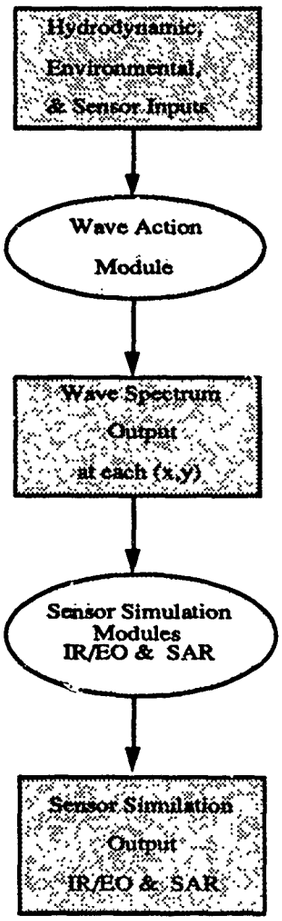

Figure 1. Flowchart for the ERIM Ocean Model (EOM).

The first processing module is the wave action module. Its inputs are the 2-D surface currents and the environmental conditions. In this module EOM integrates the nonlinear wave action equation to compute the variations in action spectral density in the presence of variable currents. It does this on a 2-D spatial and wavenumber grid.

Following the spectral processing, a description of the sensor and its resolution are input into EOM. If the sensor is a SAR, EOM uses the two-scale Bragg scattering theory to calculate the radar cross section (RCS). Next, a realization of the ocean surface is created so the SAR phase history of the ocean surface can be constructed. Then, EOM focuses the phase history and outputs the simulated SAR image of the ocean surface phenomena. Intermediate results can also be output in order to determine which physical processes were dominant in the image formation.

Before describing the inclusion of turbulence, we will review the pertinent theory—namely, the action spectral density theory. EOM's action spectral equation is a full nonlinear 2-D description of the ocean surface wave physics:

$$(c_{gx}+u)\frac{\partial N}{\partial x} - (k_x\frac{du}{dx} + k_y\frac{dv}{dx})\frac{\partial N}{\partial k_x} +$$

$$(c_{gy}+v)\frac{\partial N}{\partial y} - (k_x\frac{du}{dy} + k_y\frac{dv}{dy})\frac{\partial N}{\partial k_y} = F_s(N)$$

where c_{gx} and c_{gy} are the group velocity components, N is the action spectral density, u and v are the currents, and $F_s(N)$ is the net sum of all the known sources and sinks of wave energy. The action is related to the more familiar wave height spectrum, S, by the relation: $N = \rho\, c\, S$ where c is the phase speed and ρ is the density of water. The action spectral equation is solved in EOM by an upwind differencing scheme.

For the simulations described in this report, the net source function was assumed to be of the form discussed in detail by Lyzenga (1991):

$$F_s(N) = \Pi + \beta N - \beta_d N - \gamma N^2.$$

The terms in this equation represent, respectively, the Phillips growth mechanism,

an exponential wind growth mechanism, a viscous damping term, and a nonlinear dissipation term which is intended to incorporate the effects of wave breaking in limiting the wave growth. This equation is essentially a generalization of the Hughes (1978) formulation.

Many of the terms in the net source function are highly uncertain. We have used the exponential growth parameter suggested by Snyder et al. (1981),

$$\beta = 0.0003\,[U/c\,\cos(\phi - \phi_w) - 1]\,\omega,$$

and the viscous dissipation rate, $\beta_d = 4\,\nu k^2$, which is well known. In order to estimate the other two terms (Phillips growth and nonlinear wavebreaking) we have assumed that for wavenumbers near the spectral peak, the equilibrium spectrum is the result of an approximate balance between these two terms, and that this equilibrium spectrum has the Pierson-Moskowitz (1964) form, so that

$$\Pi = \gamma N^2_{PM}$$

where $N_{PM} = \rho\, c\, S_{PM}$ and S_{PM} is the Pierson-Moskowitz height spectrum, converted to wavenumber coordinates using a $\cos^4[(\phi - \phi_w)/2]$ azimuth dependence. This leaves one unknown parameter, γ, which may be re-written as $\gamma = (\omega k^4/\rho c)\,\gamma_o$ where γ_o is a dimensionless constant.

The total equilibrium spectrum is given by the solution of the equation $F_S(N_o) = 0$, which yields

$$N_o = \frac{(\beta - \beta_d) + [(\beta - \beta_d)^2 + 4\,\gamma\,\Pi]^{1/2}}{2\gamma}$$

This results in a wind speed dependence at large wavenumbers, the magnitude of which depends on the constant γ_o. Thus, this parameter was chosen (γ_o=1) to match the wind speed dependence of the slope variance, as observed by Cox and Munk (1954). This comparison is shown in Figure 2.

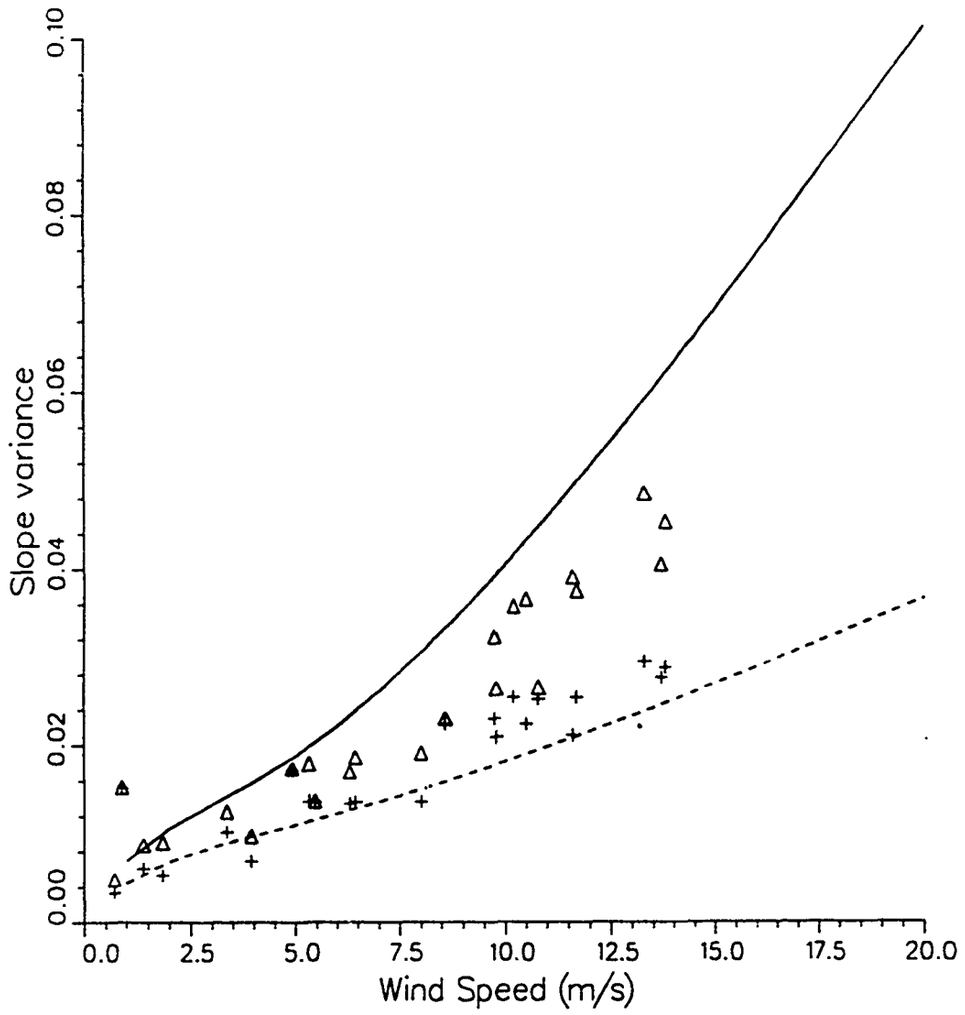

LEGEND

Up–wind component

Cross–wind component

Δ Cox & Munk data (upwind)

\+ Cox & Munk data (crosswind)

Figure 2. Comparison of Slope Variances Calculated From Spectral Balance Model to Observations of Cox and Munk (1954).

This completes the description of the action spectral theory in EOM prior to the addition of new sink terms. Additional wave energy sinks which were considered included: surfactants, turbulent scattering, and turbulent dissipation. Although surfactants are likely to be involved in some cases, the dark centerline wakes seem too ubiquitous to be explained in all cases by surfactants, which vary widely geographically. Turbulent scattering (as discussed by Phillips [1959]) was proposed as a possible mechanism and an iterative procedure was proposed for its inclusion into EOM. Finally, turbulent dissipation was chosen because it could be incorporated into EOM with relatively little difficulty. As it turned out, the turbulence levels produced in FF and DD ship types appear to produce appreciable Bragg wave reduction using this formulation.

2.2. TURBULENT DISSIPATION INCLUSION IN ERIM OCEAN MODEL

The turbulent dissipation was modeled by adding a new term to the viscous damping rate, as proposed by Milgram (1991):

$$\beta_T = 0.103 \frac{u'}{L^{1/3}\lambda^{2/3}}$$

where u' is the horizontal turbulence velocity near the surface, L is the mixing scale length, and λ is the wavelength. In terms of the turbulent dissipation, ϵ, the turbulent damping rate is: $\beta_T = 0.10\,\epsilon^{1/3}\,k^{2/3}$. Then β_T was added to β_d and

$$F_S(N) = \Pi + \beta N - \beta_d N - \gamma N^2$$

was solved for the modified equilibrium. The effect of turbulence on the spectrum is shown in Figure 3. The form of β_T is similar to that used by DTI in their turbulence model except for the magnitude of the numerical constant. A comparison between the two formulations is contained in Appendix A.

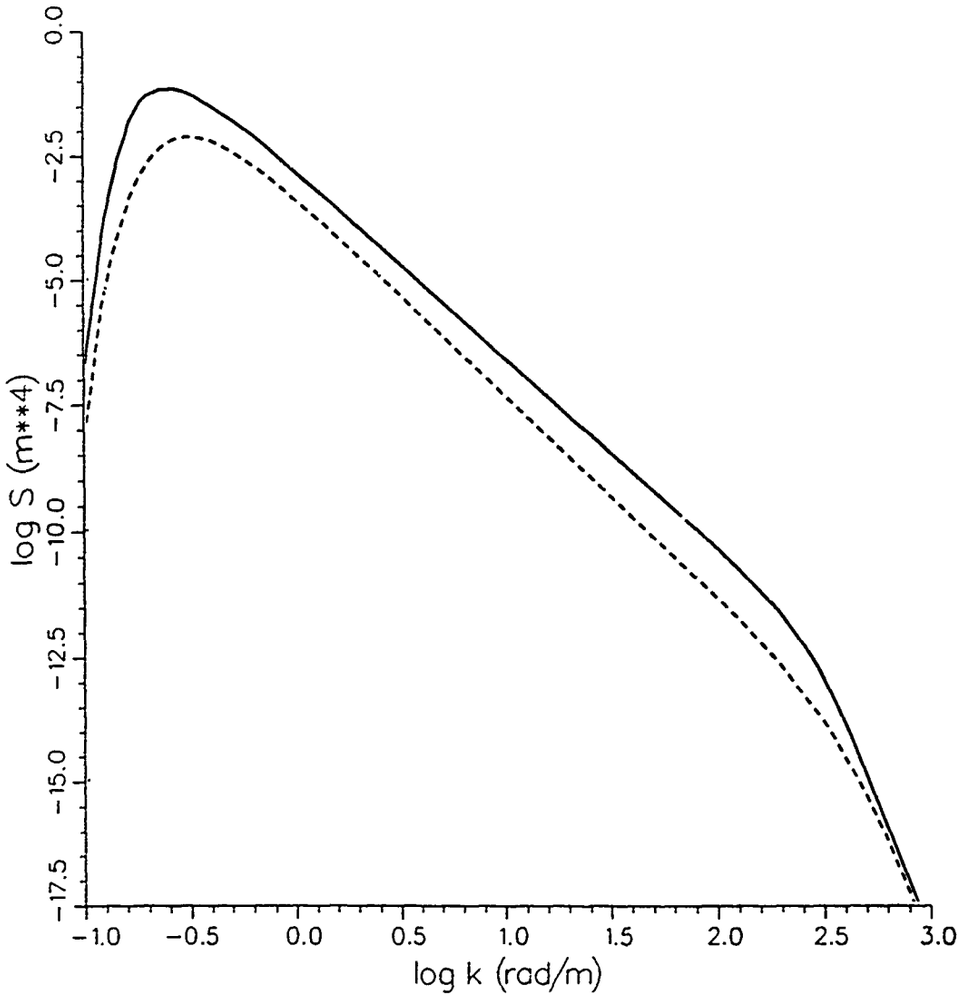

Figure 3. Equilibrium Wave Height Spectrum With (---) and Without (——) Turbulent Dissipation.

The relaxation rate is defined by:

$$\beta_r = -F_s'(N_o) = [(\beta - \beta_d)^2 + 4\,\omega\,\gamma\,\Pi]^{1/2}$$

where β_d includes the turbulent dissipation. The effect of turbulence on the relaxation rate is shown in Figure 4. The net effect of turbulence, as shown in Figures 3 and 4, is the reduction of the action spectral density due to the turbulent dissipation. The analysis in the next section will address the effects of turbulence on the radar cross section (RCS). The effects on the RCS of other variables such as wind speed, wind direction, incidence angle, and track aspect will also be included.

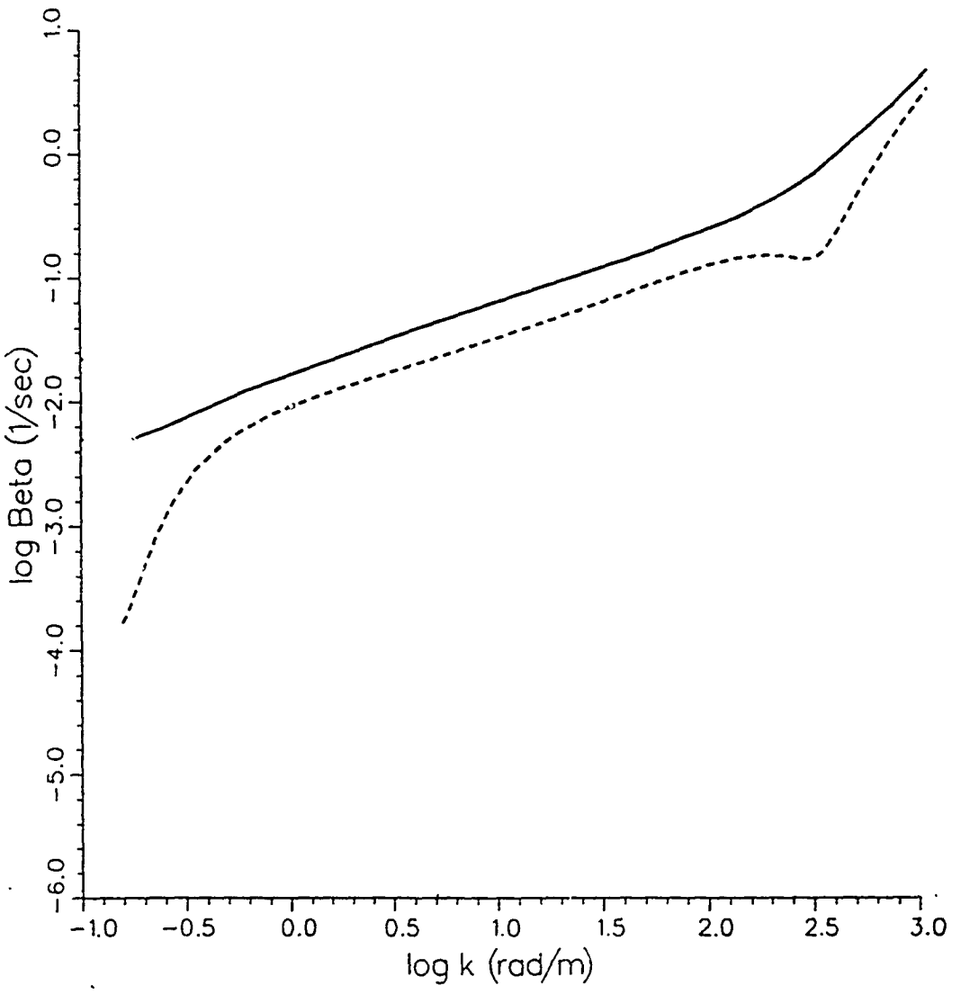

Figure 4. Relaxation Rate With (——) and Without (----) Turbulent Dissipation.

2.3 SENSITIVITY ANALYSIS USING 1-DIMENSIONAL RUNS

Typically, more than one environmental parameter changes between the experimental cases. Therefore, it was difficult to isolate the physical cause of changes to the RCS profile. To better understand the importance of the environmental and ship-induced variables, 1-D EOM simulations were performed varying only 1 parameter at a time. DDG Case 4 (see Table 1 in Section 3.1) was used as the baseline—the parameters were: 9 kts Crosswind, 50° Incidence Angle, Azimuth Look, and Snyder Beta. A RCS crosswake cut at 1000 meters downstream is shown in Figure 5. For analysis purposes the RCS profile of the centerline wake was characterized by its width, modulation depth, and degree of small scale features. This characterization is shown schematically in Figure 6.

A description of the RCS sensitivity to the various parameters is given below.

Turbulence

The effect of turbulence was as anticipated—an almost linear increase in modulation depth with turbulent damping rate. Note, a 50% increase of the damping rate can be achieved by doubling the constant of proportionality in the damping formula or increasing the dissipation rate, ϵ, by a factor of 8. In other words, the modulation depth is not sensitive to the dissipation rate.

Currents

Leaving turbulence on, but turning the surface current off, gives a purely negative modulation of the RCS. The modulation due to the surface current is predominantly the high frequency structure which is superimposed on the turbulence-induced trough.

Wind Speed

The wind speed has a moderate effect on the RCS modulation depth. The RCS decreases with increasing wind speed.

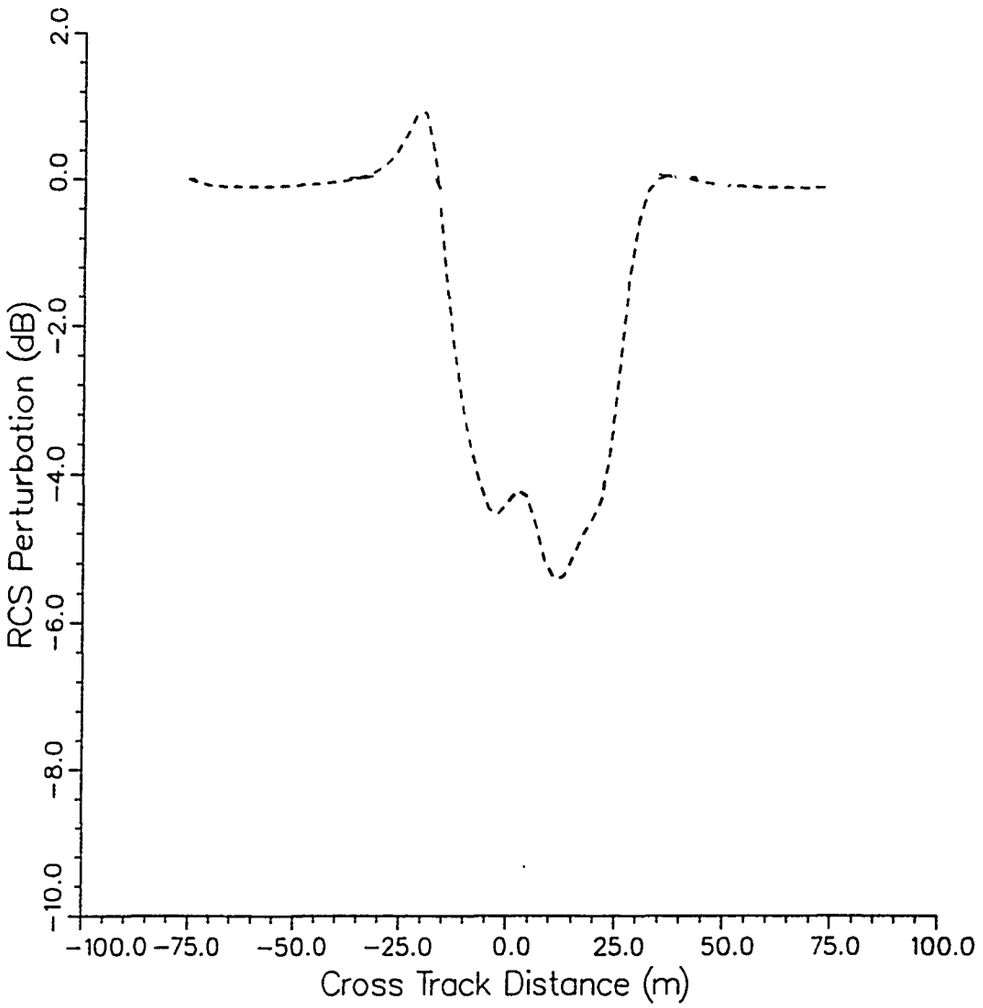

Figure 5. Crosswake Cut for the Baseline Case.

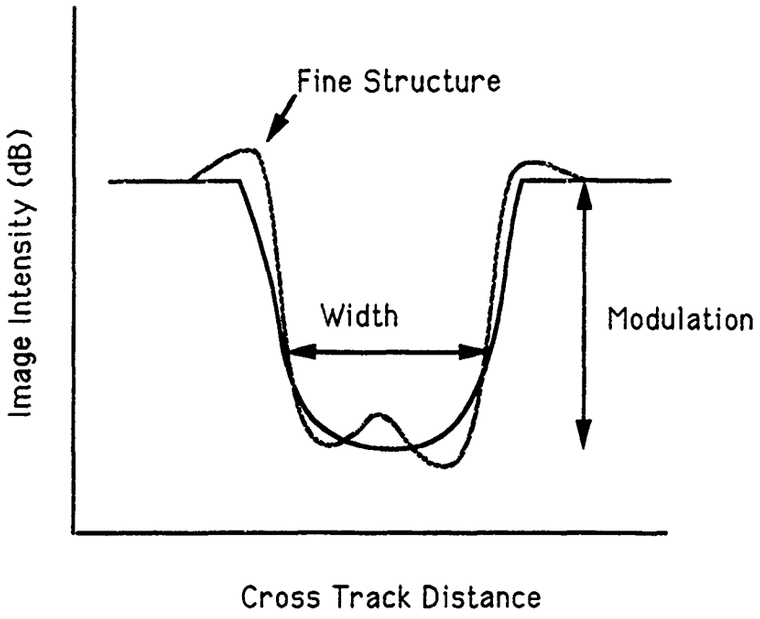

Figure 6. **Characterization of Crosswake Cut in Terms of Width, Modulation Depth, and Fine Structure.**

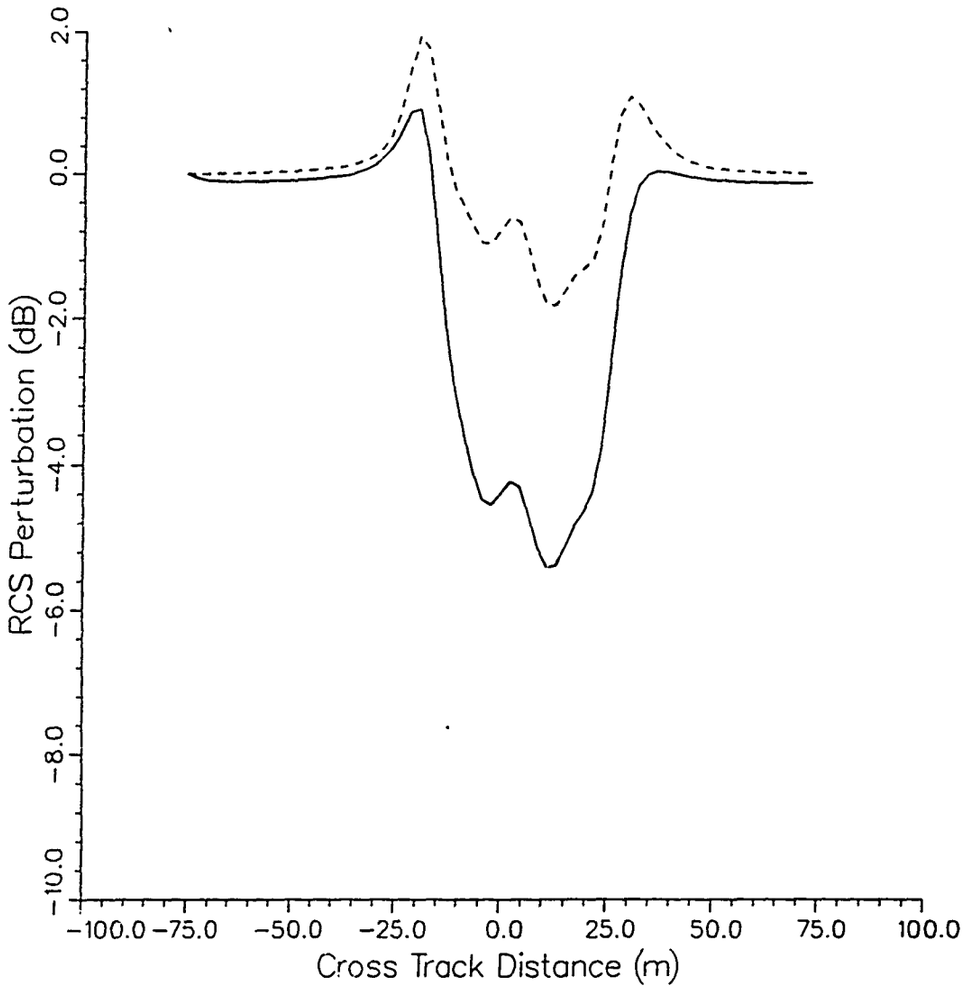

Figure 7. Crosswake Cut With and Without Turbulence.

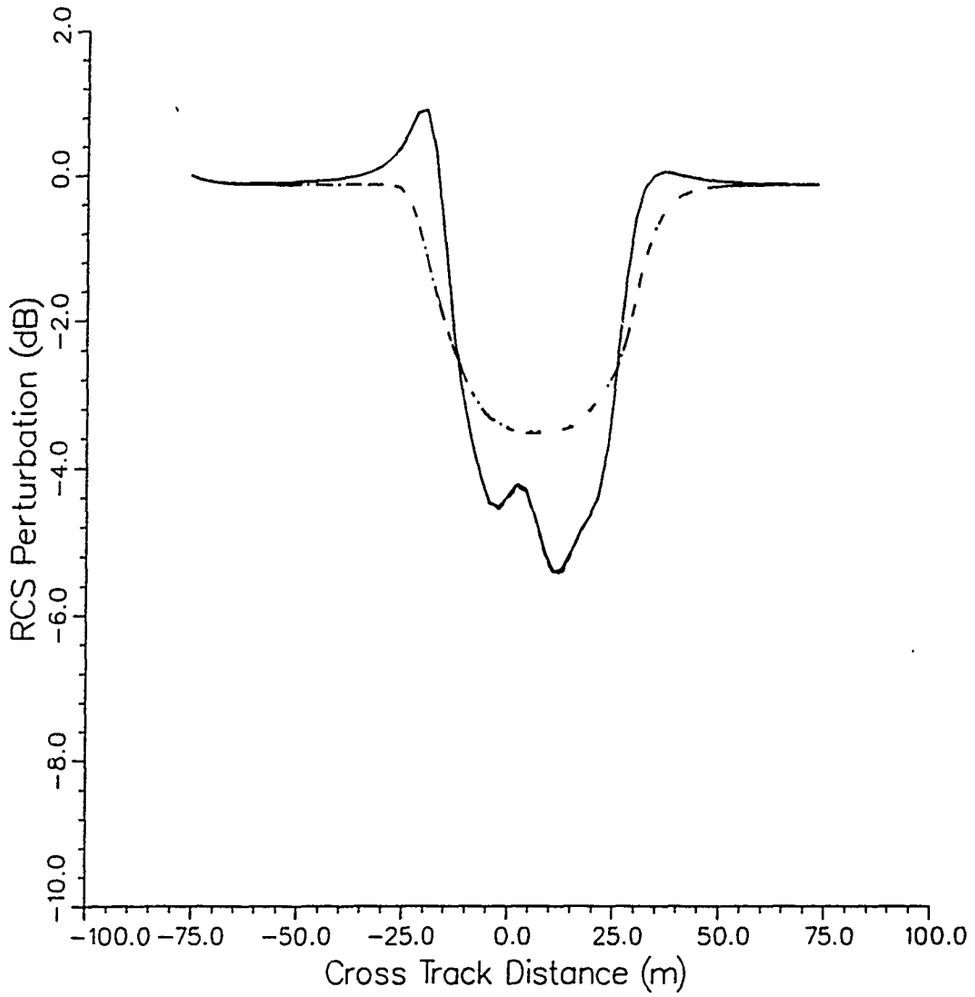

Figure 8. Crosswake Cut With and Without Surface Current.

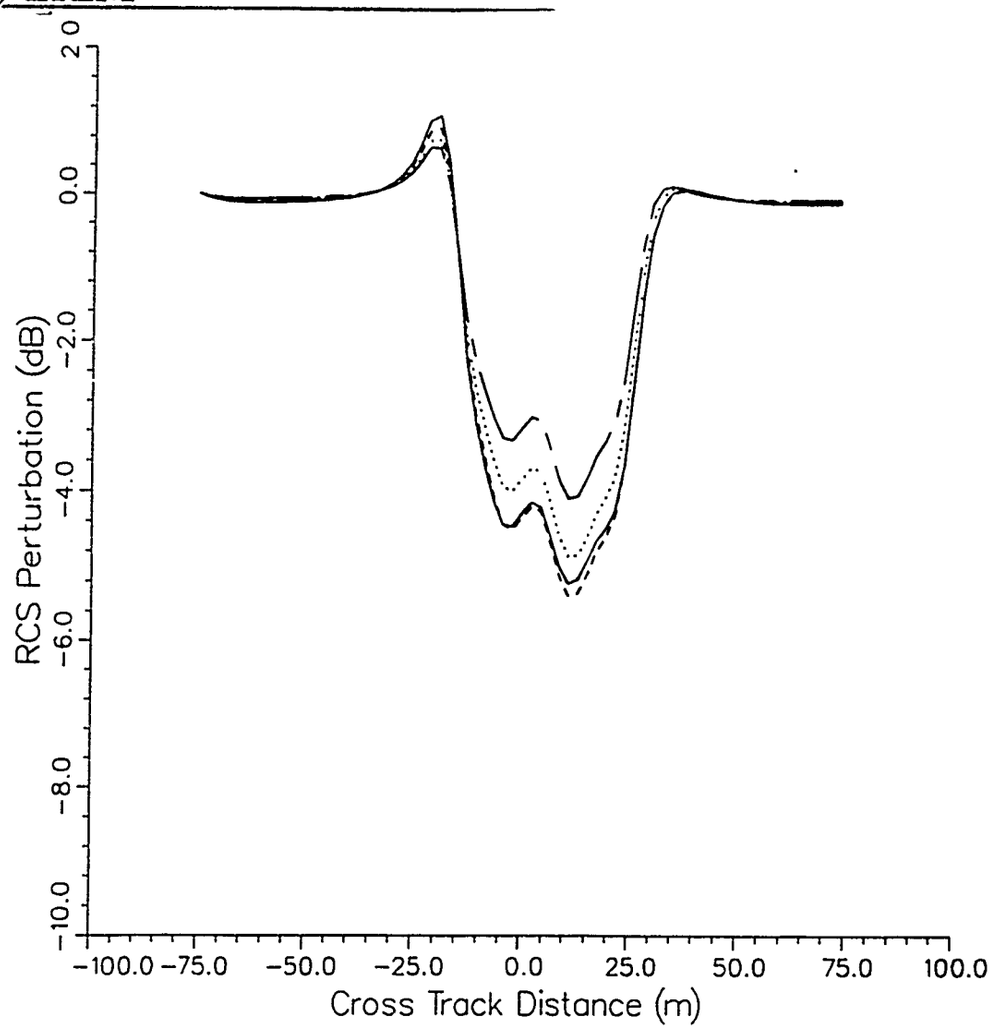

Figure 9. Crosswake Cut with Varying Wind Speed.

Wind Direction

The wind direction has an even greater effect than the wind speed on the modulation depth. The modulation depth is greatest for along track winds and least for cross track winds. Recall that the look direction for the baseline case was for an azimuth traveling wake. This wind direction sensitivity may not be universal for all look directions.

Incidence Angle

It is well known that the incidence angle has a great effect on the background RCS. However, it has almost no influence on the wake modulation when the incidence angle variation is between 30 and 60 degrees.

Track Aspect : Range-Azimuth

Note the wider profile for the range case; it is due to the smearing caused by the spread of radial velocities of the Bragg scatterers. For the azimuth case, the smearing is along the direction in which there is slow variation of the RCS so the smearing has little effect on the profile width.

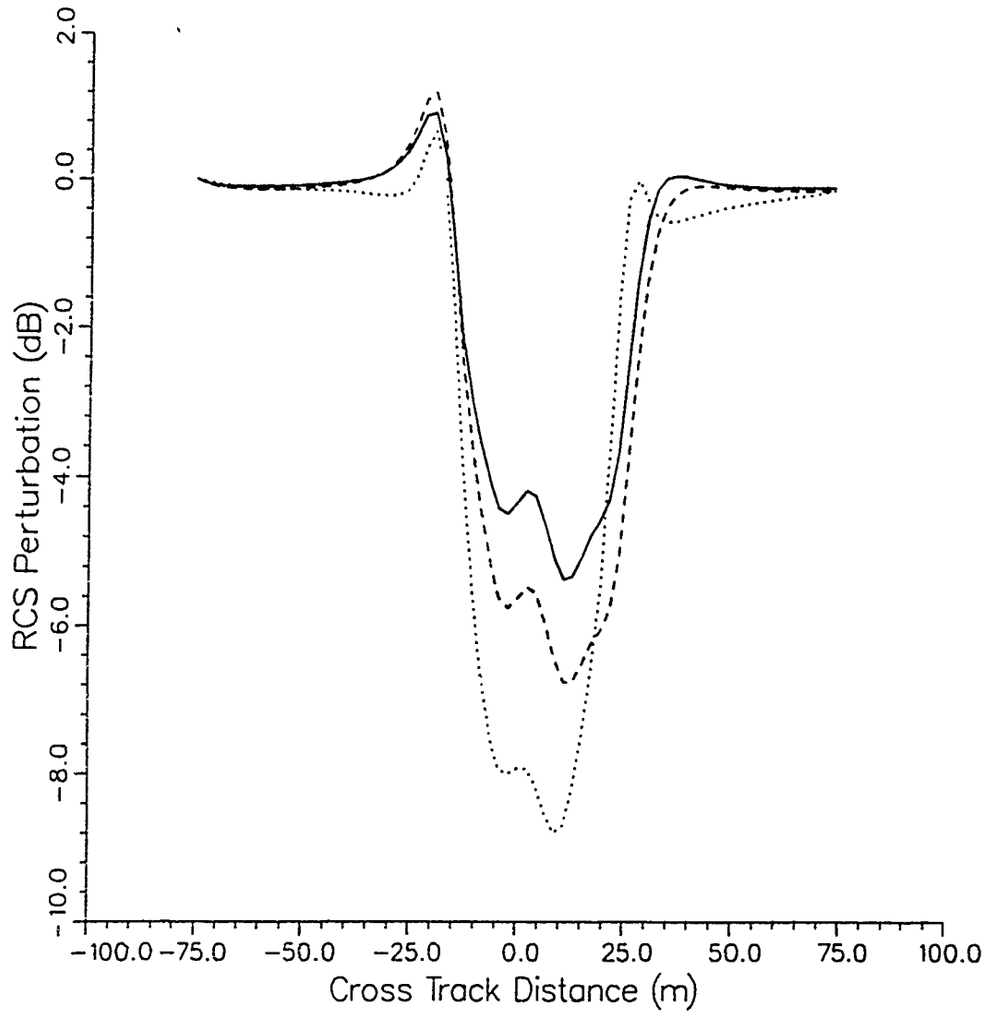

Figure 10. Crosswake Cut with Varying Wind Direction.

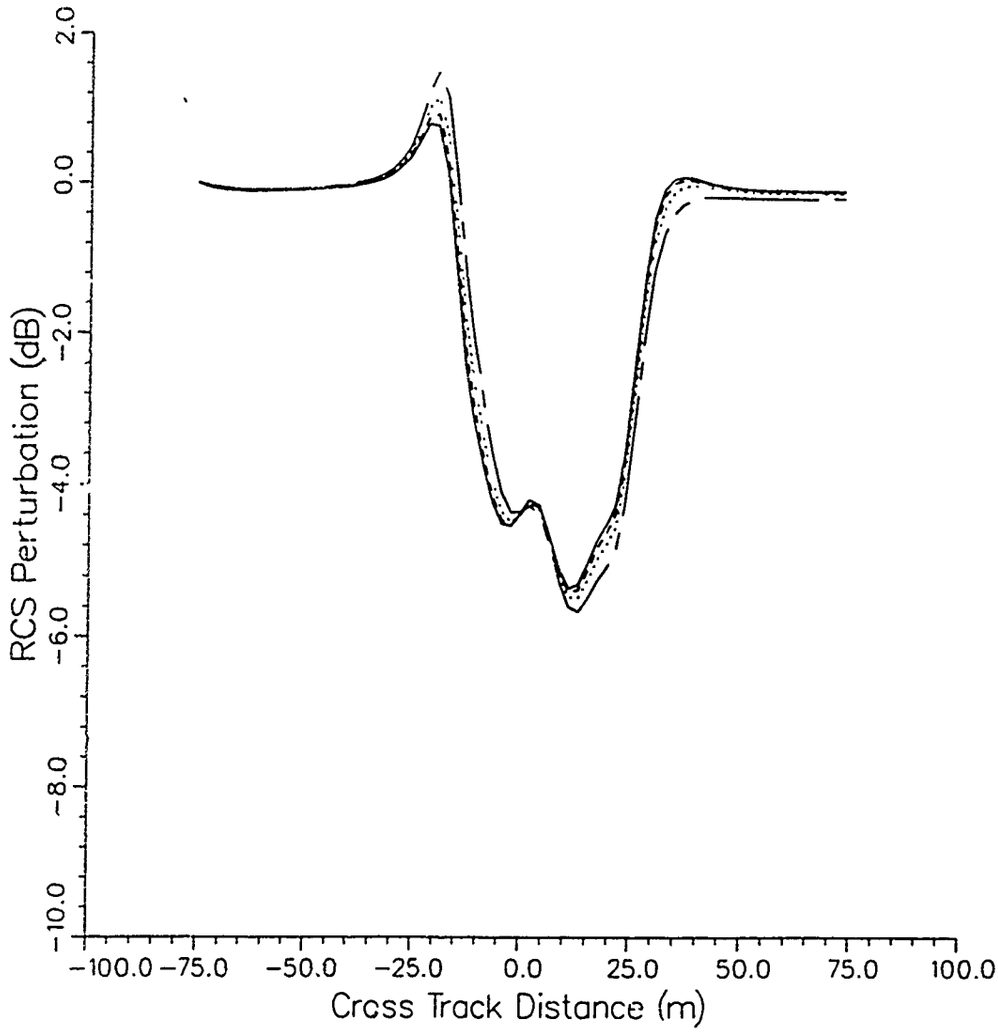

LEGEND

60 degrees

50 degrees

40 degrees

30 degrees

Figure 11. Crosswake Cut with Varying Incidence Angle.

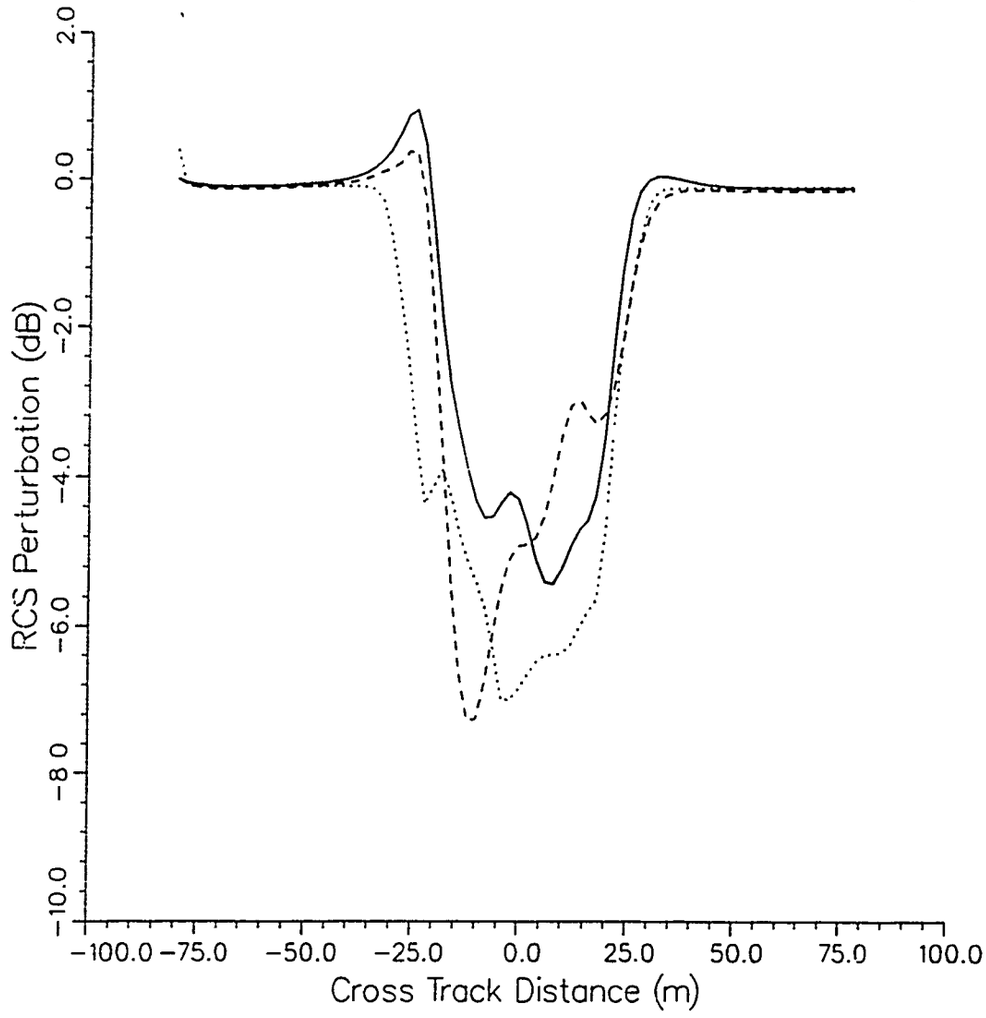

Figure 12. Crosswake Cut with Varying Track Aspect.

The results of the sensitivity analysis are summarized in Figure 13. It was found that the centerline wake width depended most strongly on the width of the turbulent dissipation region and to a lesser extent on the current profile. The modulation depth was most sensitive to the turbulent damping, wind speed, and wind direction. Finally, the high spatial frequency modulations in the centerline wake were most sensitive to the track aspect, wind direction, and current amplitude.

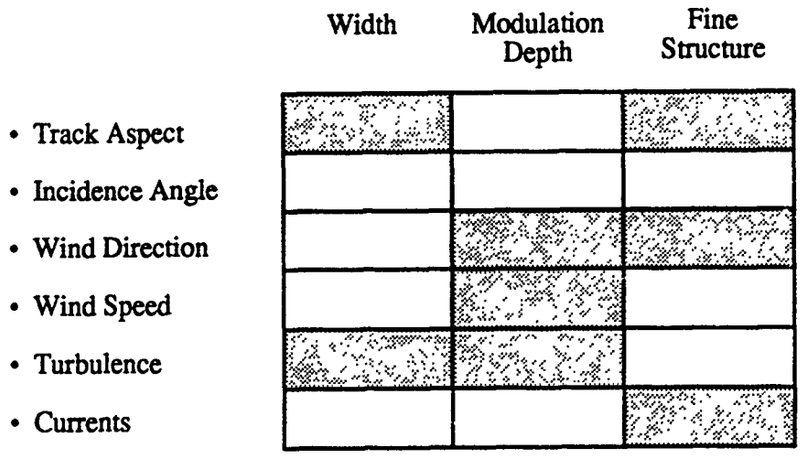

Figure 13. Results of Sensitivity Study. Shaded Regions Indicate High Sensitivity.

3.0 ERIM OCEAN MODEL RUNS

The purpose of this section is to discuss EOM's contribution to the end-to-end simulation of the centerline shipwake cases. All the cases were run with the turbulent dissipation included in EOM as described in the previous section.

3.1. INPUT HYDRO AND ENVIRONMENTAL DATA

The inputs to EOM consisted of two types: 1) 2-D surface current and dissipation files and 2) input parameters which describe the environmental conditions and the sensor type. The inputs to EOM are shown in the next two tables which are separated by ship type into: DDG (Table 1) and FF & FFG (Table 2).

Table 1. Centerline Shipwake Inputs for DDG Cases 1-7

Case	1	2	3	4	5	6	7
Run-Pass	222-1 &5	222-2 &4	746-2	746-4	746-5 &3	746-1	212-3
Wind							
Speed Type	Hi	Hi	Hi	Hi	Hi	Low	Hi
Speed (kts)	22	22	7.5	9.5	9./10.	6.	22
Direction	050°	050°	295°	310°	290°/305	300°	50°
Type	Along	Along	Cross	Cross	Cross	Any	Any
Ship							
Type	DDG	DDG	DDG	DDG	DDG	DDG	DDG
Velocity (kts)	18	18	18	18	18	18	18
Heading	55°	55°	210°	210°	210°	210°	205°
SAR							
Heading Type	Az	Az	Rg	Az	Az/30	Rg	Az
Heading	55°	235°	120°	210°	30°/45°	120°	25°
Velocity (m/s)	125/135	128	131	142	142	135	129
Altitude (m)	3028/3027	3028	3063	3087	3087	3094	3134
Inc. Angle	48°/53°	36°/39°	20°	50°	27°/26°	31°	44°/48°

Table 2. Centerline Shipwake Inputs for FF and FFG Cases 8-16

Case	8	9	10	11	12	13	14	15	16
Run-Pass	736-1	736-2	776 &2	776-4 &5	776-3	766-1	766-1	766-3	766-3
Date	1-26	1-26	2-1	2-1	2-1	1-31	1-31	1-31	1-31
Wind (new values)									
Speed Type	Hi	Hi	Hi	Hi	Hi	Low	Low	Low	Low
Speed (kts)	18	18	9./9.	8./8.	8.5	8.	8.	8.0	8.0
Direction	000°	005°	245°/250°	275°/280°	270°	240°	240°	250°	250°
Direction	Along	Along	Cross	Cross	Cross	Any	Any	Any	Any
Ship									
Type	FFG	FFG	FF	FF	FF	FF	FFG	FF	FFG
Velocity (kts)	18	18	18	18	18	18	18	18	18
Heading	210°	210°	210°	210°	210°	210°	210°	210°	210°
SAR									
Heading Type	Rg	Rg	Rg	Az	30	Rg	Rg	30	30
Heading	120°	120°	120°	030°	045°	120°	120°	045°	045°
Velocity (m/s)	117	115	126/123	136/127	137	128	128/127	120	120
Altitude (m)	3045	3044	3069/ 3067	3059/ 3064	3060	3089	3089	3085	3085
Inc. Angle	29°	46°	46°	48°/50°	23°	52°	46.7°	21°	21°

The 2-D surface currents and turbulent dissipation were calculated by SAIC's FASTWAKE program. The environmental and sensor input parameters were chosen to match the ONR data set. When two values are given in the tables, the average was used. The SAR wavelength (L-band) and polarization (VV) were the same for all cases. The wind directions in the table were converted into the wind directions with respect to the ship track (EOM's angle convention). These are best described by a schematic overhead view of the shipwake as shown in Figure 14.

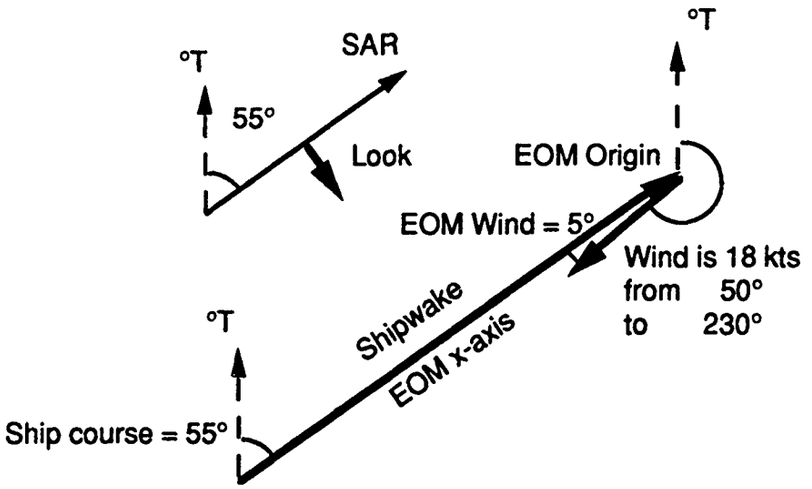

Figure 14. Plan View of Shipwake for Case DDG-1.

Similarly, EOM's SAR look direction is defined as the look vector's angle with respect to the X-axis (counter-clockwise). The output SAR-RCS images which were used for matched filters had 2.16 m sample spacing in the cross-track direction and 8.64 m sample spacing in along-track direction.

3.2 PRODUCTION METHODS

The production of centerline wake images began with the Dummy Run which initiated the coordination between the organizations. The production flowchart showing the organizations and computer programs is shown below.

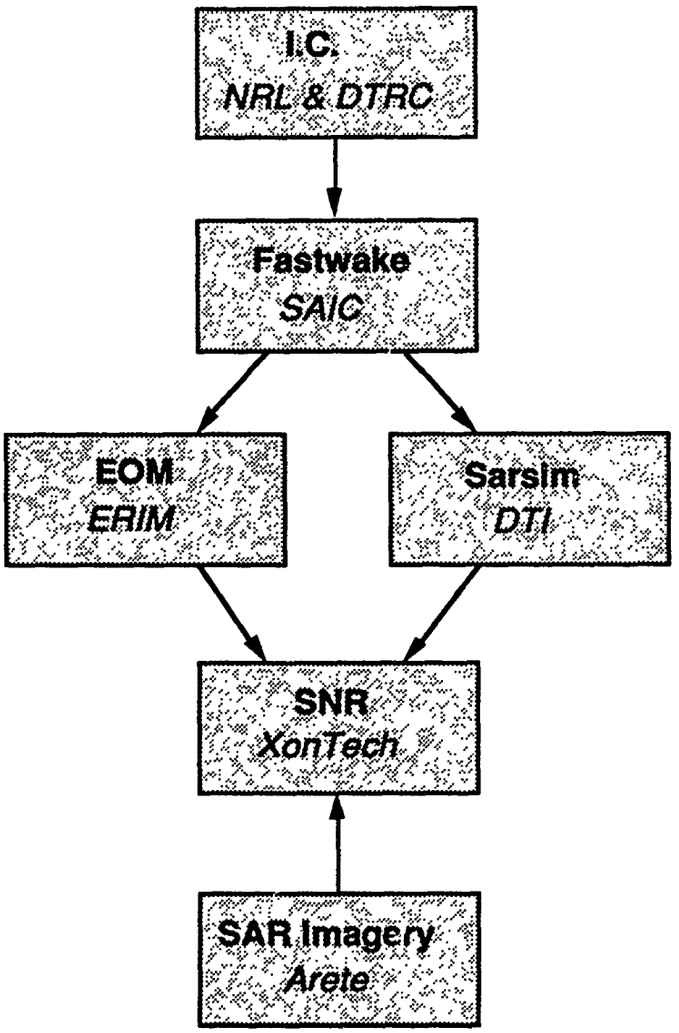

Figure 15. Centerline Shipwake End-to-End Production Flowchart.

After the Dummy Run was completed SAIC sent the actual surface current and turbulence data via the Internet. The surface currents (cross wake and along wake components) and turbulent dissipation included two versions for three ship types—FF, FFG, and DDG. The two versions of the current and dissipation files for each ship type corresponded to improvements in SAIC's FASTWAKE code. The 2-D files were

transmitted in ASCII text form and were converted back into numeric form with a utility program which also reduced the crosswake spacing by a factor of 4 via averaging. The 2-Dcurrent and dissipation files were previewed before being input into EOM.

Separate EOM batch files were created for each of the 16 cases in Tables 1 & 2. An example of the batch file which executed the programs is shown in Appendix B. Each EOM run took roughly 3-4 cpu hours/run on the Multiflow Trace (a parallel processing mini-supercomputer). Although EOM uses a fixed grid, its convergence test at the end of each iteration of the solution meant that run times were not constant; they were longer for stronger surface currents or wave trapping conditions.

EOM interpolates wave characteristics between the grid points on its X-Y-k-ϕ mesh. This results in a faster code, but inaccuracy can result if the solution changes at a higher angular or wavenumber frequency than the grid spacing. To test the effects of this, EOM was run with twice and half the number of wavenumbers (k) and angles (ϕ). 48 wavenumbers and 12 angles were used because there was no change in the solution when the spacing was halved.

The largest file that EOM makes is the 2-D spectrum at each X-Y grid point. It was archived so that other frequencies could be re-run easily. Also, EOM intermediate and final products were backed up on 8 mm tapes. The data products are described by their suffixes:

.eom	The eom file which has the input parameters
.cmd	The command line simply starts a shell off csh < filename.cmd > filename.log &
.eql	Output from RSLWAVE
.dat	Output from RSLWAVE
.spc	Output from RSLWAVE
.pmv	Mean radial velocity, output from psar option
.pvv	Radial velocity variance, output from psar option
.prc	Radar cross section of wake only, output from psar option
.pii	Cross section of combined wake and wave clutter

Normally, EOM produces the finished product—a focussed SAR image. Since the SAR image is produced from a phase history, it inherently has speckle. This was not desired for the matched filter application. Another ERIM program—SOS—produces an RCS image including velocity translation and smearing effects, but without speckle. The two programs EOM and SOS were used in sequence to produce the desired matched filter. The production sequence was: the output products from EOM (RCS, mean radial velocity, and radial velocity variance) were input into SOS and the RCS matched filter was output.

The speckle-less RCS images were converted to an ASCII text file and put on a 3.5" floppy and sent to XonTech along with a description of the data format and geometry. In the first phase 32 SAR-RCS images (without speckle) were sent to XonTech corresponding to 16 cases with 2 betas for each case. The two betas (Plant and Snyder) had similar growth rates but relaxation rate was much greater for Plant's beta which caused a small RCS modulation. In the second phase runs were made at C-band for cases 14 and 16. The C-band runs were economically generated because the time-intensive portion of EOM is not dependent on radar wavelength. The previous EOM runs were retrieved from the archived tapes and the final wavelength dependent portions of EOM and SOS were run. Finally, copies of the matched filters were archived at ERIM.

3.3. OUTPUT PRODUCTS

The 2-D falsecolor RCS images for Cases 1-16 using Snyder's beta are shown in Appendix C. Using the 1-D sensitivity results as a guide, the 2-D runs were compared to others (of the 16 cases) with similar parameters. The results are summarized here.

Case 1. The red bright edge on the windward side is due to the converging cross track current on the outer edge of the wake. The bright edge on the leeward side is less intense because the wave relaxation rate is low causing the 'memory effect' of the lower spectral density inside the wake.

Case 2. The red bright edge is on the windward side. Note that the wind direction is from the other side than in Case 1.

Case 3. The track aspect dependence on the width of the centerline wake is shown by comparing this Case (range aspect) with Case 4 (azimuth aspect). For the range aspect the wake width is 35% wider at midwake than the wake width of the azimuth aspect.

Case 4. The wind aspect dependence of the modulation depth is shown by comparing this Case (cross track) with Case 7 (along track).

Case 5. The incidence angle dependence is shown to be weak by comparing this Case (incidence angle = 27°) with Case 4 (incidence angle = 50°). The 180° rotation between the 2 images is due to differences in look direction and parallel and anti-parallel Ship-SAR relative heading.

Case 6. The conditions for this Case are similar to Case 3 and therefore the two images are very similar.

Case 7. The wind aspect dependence of the modulation depth is shown by comparing this Case (along track wind) with Case 4 (cross track wind). The along track wind Case 7 has a greater modulation depth than the cross track wind Case 4.

Case 8. The wind speed dependence on modulation depth is shown by comparing this Case with Case 14. The lower wind speed case has a greater modulation depth than the higher wind speed case.

Case 9. The conditions for this Case are nearly the same as Case 8 and therefore the two images are very similar.

Case 10. The track aspect dependence on the width of the centerline wake is shown by comparing this Case with Case 11. For the range aspect the wake width is 35% wider than for the azimuth aspect Case.

Case 11. The track aspect dependence on the width of the centerline wake is shown by comparing this Case with Case 10. For the range aspect (Case 10) the wake is 35% wider than the azimuth aspect (Case 11).

The conditions are similar to Case 15. A faint bright edge on the windward side of the wake is visible.

Cases 13 and 14. The ship-type dependence of the centerline wake is shown by comparing Case 13 with Case 14. Both ships (FF and FFG) were in the same SAR image, but at different incidence angles. It was shown on Cases 4 and 5 that incidence angle effects are small when the intensity modulations are measured with respect to background. The ship type variation is: the FFG had a smaller modulation depth due to its smaller turbulence level and also a smaller high frequency modulation due to its smaller cross track current velocity.

Cases 15 and 16. The ship-type dependence of the centerline wake is shown by comparing Case 15 with Case 16. Both ships (FF and FFG) were in the same SAR image, but at different incidence angles. The ship type variation is: the FFG had a smaller modulation depth due to its smaller turbulence level and also less high frequency modulation due to its smaller cross track current velocity.

4.0 CONCLUSIONS AND RECOMMENDATIONS

The results of this study demonstrate the ERIM Ocean Model's contribution to the end-to-end simulation of the centerline shipwake including the effects of turbulence. The inclusion of turbulent dissipation into EOM was shown to be a realistic explanation of the predominantly 'dark' modulation associated with the centerline shipwake. However, the simulated shipwakes were significantly narrower than the experimental data, leading to the conclusion that the hydrodynamics modeling of the current and dissipation widths needs further improvement.

A centerline wake sensitivity study was performed using EOM. Specifically, the sensitivity of the wake width, 'depth', and fine-structure on the ship type, track aspect, wind direction, wind speed, and turbulence were determined using the DDG (Case 4) conditions as the baseline. The wake width was most dependent on the turbulent dissipation width; and, there was some wake broadening due to the surface velocity variance when the wake was viewed range-traveling. The modulation depth was most sensitive to turbulent damping, wind speed and wind direction. The high-frequency spatial structure of the wake was most sensitive to the track aspect, wind direction, and current pattern.

The end-to-end model validation stressed the comparison of the matched filter with the experimental data. This led to a validation metric which was predominantly affected by the shape of the wake. However, the EOM sensitivity study suggests that the wake depth and hi-frequency spatial modulation should also be considered in the validation metric. Since there are sensitivities in those observables, their use would better validate the modeling and give additional discrimination for future identification processing. In particular, this study suggests that additional simulations (and field data) are required for X-band and other SAR aspects to adequately validate the simulation models.

5.0 ACKNOWLEDGEMENTS

This work was sponsored by the Office of Naval Research (ONR) under Contract Number N00014-90-C-0071. The technical monitor for this effort was Dr. David Johnson. The authors would like to thank George Innis of SAIC, Dan Michelson of DTI, and Curt Harkless of XonTech for their cooperation on this work.

6.0 REFERENCES

Cox, C. and W. Munk, Statistics of the sea surface derived from sun glitter, *J. Mar. Res., 13*, 198-227, 1954.

Hughes, B. A., The effect of internal waves on surface wind waves, 2, Theoretical analysis, *J. Geophys. Res., 83*, 455-465, 1978.

Kitaigorodskii, S. A. and J. L. Lumley, Wave-turbulence interactions in the upper ocean. Part I. The energy balance of the interacting fields of surface wind waves and wind-induced three dimensional turbulence, *J. Phys. Ocean., 13*, 1977-1987, 1983.

Lyzenga, D. R. and J. R. Bennett, Full-spectrum modeling of synthetic aperture radar internal wave signatures, *J. Geophys. Res., 93*, 12345-12354, 1988.

Lyzenga, D. R., Interaction of short surface and electromagnetic waves with ocean fronts, *J. Geophys. Res., 96*, 10765-10772, 1991.

Milgram, personal communication, 1991.

Olmez, H.S. and J.H. Milgram, Attenuation of water waves by turbulence, *MIT Dept. of Ocean Engineering Report, 39 pp.*, 1989.

Phillips, O.M., The scattering of gravity waves by turbulence, *J . Fluid Mech., 5*, 177-192, 1959.

6.0 REFERENCES (CONCLUDED)

Phillips, O.M., *The Dynamics of the Upper Ocean*, 1st paperback ed., 336 pp. Cambridge University Press, New York, 1980.

Phillips, O.M., Spectral and statistical properties of the equilibrium range in wind generated gravity waves, *J. Fluid Mech., 156*, 505-531, 1985.

Pierson, W.J., and L. Moskowitz, A proposed spectral form for fully developed seas based on the similarity theory of S. A. Kitaigorodskii, *J. Geophys. Res., 69*, 5181-5190, 1964.

Plant, W.J. A two-scale model of short wind-generated waves and scatterometry, *J. Geophys. Res., 91*, 10735-10749, 1986.

Snyder, R.L., F.W. Dobson, J.A. Elliott, and R. D. Long, Array measurements of atmospheric pressure fluctuations above surface gravity waves, *J. Fluid Mech., 102*, 1-59, 1981.

APPENDIX A. COMPARISON OF ERIM AND DTI TURBULENCE MODELS

Milgram's model was simple to implement in EOM because the turbulent dissipation rate is similar in form to the viscous dissipation rate already included in the right-hand-side of EOM's wave action equation. DTI's turbulent dissipation rate was the same functional form as Milgram's but there was a difference of 100 in the numerical coefficient. Although some disagreement between the turbulent dissipation rates is expected because turbulence-theory derivations are not precise, the difference was so large that its cause was investigated and the results are discussed below.

Milgram's turbulent dissipation rate

Milgram's turbulent dissipation rate is:

$$\beta_T = 0.103 \frac{u'}{L^{1/3}\lambda^{2/3}}$$

where u' is the horizontal turbulence velocity near the surface, L is the mixing scale length, and λ is the wavelength . The theoretical justification of Milgram's result is described in Kitaigorodskii and Lumley (1983) as follows: turbulence can cause surface wave energy loss due to turbulence-induced downward convection of wave energy. A key point is that the energy of the surface wave extends $1/k = \lambda/2\pi$ below the ocean surface. Any interchange of fluid elements above or below k^{-1} effectively destroys wave energy. Milgram points out that his experimental results are consistent with the Kitaigorodskii and Lumley theory but he suggests that more experiments are necessary to prove the theory. The reason for Milgram's use of 'consistent with' rather than 'confirms' is due to the experimental setup of Milgram which left some key variables of the Kitaigorodskii and Lumley theory unmeasured.

Olmez and Milgram's (1989) experimental result is a curve of turbulence-induced decay rate, β_T, versus turbulent mixing length, M. It shows that β_T and M are linearly proportional. The constant of proportionality is 0.103. The turbulent mixing rate is the right hand side of the turbulent dissipation equation. But it is confusing; u' is the RMS horizontal turbulence velocity near the surface, whereas the Kitaigorodskii and Lumley paper implies that vertical motion causes the dissipation. It turns out that Milgram only

measured the horizontal turbulent velocity. A relation between the horizontal and vertical turbulent RMS velocities is required to determine the turbulent damping rate from the measured quantities.

The derivation is as follows. The mixing rate is proportional to $M = \langle w' \rangle k^{-1}$, where $\langle w' \rangle$ is the mean vertical velocity due to turbulence and $k^{-1} = \lambda/2\pi$ is the thickness of the surface wave kinetic energy layer. The average velocity is needed because w' is not constant. It is zero at the surface and isotropic ($\langle w' \rangle = \langle u' \rangle$) by the time the depth z=L is reached. w' has been experimentally determined to vary as $z^{1/3}$. In other words:

$$w' = u' (z/L)^{1/3} .$$

Since w' is zero at the surface and not equal to u' until z=L, the average value of w' will be less than u'. The following graph shows the relation between kinetic energy and w' as a function of z.

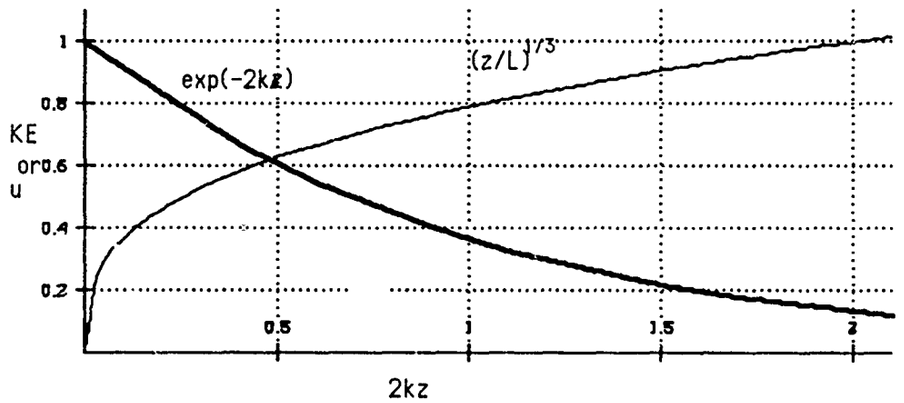

Then the average value of w' is accomplished by averaging the local flux of kinetic energy with z.

$$\langle w' \rangle = \frac{u'}{k^{-1}} \int_0^{k^{-1}} \left(\frac{z}{L}\right)^{\frac{1}{3}} e^{-2kz}\, dz = \frac{3}{4} u' \, e^{-2} \left(\frac{k^{-1}}{L}\right)^{\frac{1}{3}} + \ldots$$

This gives the constant in the turbulent damping equation at the beginning of the Appendix. It is $3/4\ e^{-2}\ (2\pi)^{1/6} = 0.137$ which is remarkably close to the experimental value. This is obviously fortuitous, but it lends credence to the physical effect that the vertical turbulent velocity is much smaller than the horizontal turbulent velocity near the ocean surface.

It is clear why more experiments are needed to prove the theory. The actual vertical turbulent velocity as a function of z must be measured to verify the downward convection of wave energy by turbulence and compare this with the wave damping caused by turbulence. Note, Kolmogorov's law was not used in the preceding derivation. Instead, the turbulence was taken to be anisotropic (at least until $z > L$). This contrasts the DTI formulation given next.

DTI Turbulence Dissipation Rate

The DTI turbulent damping rate is based on the 'classic' treatment where a strict analogy is made between kinematic viscosity and turbulent viscosity and Kolmogorov's law is used. The effect is that the viscosity is assumed to work directly on the waves of interest. There is an assumption of isotropic turbulence. The results are still qualitative; the constants must be experimentally determined. Richardson's law is invoked because it describes the horizontal diffusion of dye near the ocean surface for scales from meters to tens of kilometers. Richardson's law is a consequence of Kolmogorov's law, although it was discovered first. The length scale is taken to be $1/k_B$ which is justified on the grounds that only eddies smaller than L contribute to diffusivity. In contrast, it appears that the observations of Milgram are that the large eddies dominantly transport (in downward direction).

Next, the constant, a=0.05, is derived from observations of horizontal spreading of dyes and the isotropic assumption. The result is a turbulent damping rate which is about 100 times greater than Milgram's.

Conclusion

The DTI dissipation rate is based on Kolmogorov's model with the constant derived from experimental horizontal diffusion of dyes and not from explicit wave-

turbulence interaction.

Milgram's damping rate is almost entirely empirical but it is based on wave damping observations. Another difference is the assumption that vertical mixing is different than horizontal mixing due to the boundary effect at the ocean surface. The anisotropic turbulence assumption of Milgram is the main cause of the factor of 100 difference between his turbulent damping rate and DTI's.

APPENDIX B. A SAMPLE EOM AND SOS BATCH FILE

A typical EOM parameter file is shown below. Comments to the right of inputs are not part of the EOM file.

```
; Simulation type and output filename
;
SIMTYPE=general                    General for current file input
HYDROFILE=FFG                      All inputs will have filename 'fast'
;
; Grid dimensions in X and Y
;
NX=300                             Innis test file has nx=300
NY=1                               Innis test file has ny=128
;
; Grid dimensions in WAVENUMBER and ANGLE
;
NK=48
NP=12
;
; Min and Max wavelength of small scale waves (m)
;
WLMIN=0.010                        Defaults is good for low winds
WLMAX=50.000                       Should be 10 times wind speed
;
; Surfactant pressure (dynes/cm)
;
P0=0.000                           No surfactant
;
; Wind speed (m/s) and wind direction (deg)
;
WNDSPD=5.000                       19 kts = 5 m/s is nominal  low speed
WINDIR=117.000                     For 1-D (transpose)  207° for 2-D
;
; Amplitude (m) and wavelength of long wave (m)
;
AMPLW=0.000                        Only pertains in LW case
WVLNLW=00.000                      Only pertains in LW case
;
; Current amplitude (m/s) IW double hump case
;
UHUMP=0.000                        Only pertains in IW case
;
; Doppler velocities (m/s) in X and Y
;
UDOPLR=0.000                       This causes the pattern to translate at
```

```
                                        Uniform velocity
VDOPLR=0.000                            Similar to previous only in y-direction
;
; Water depth
;
DEEP=.True.                             Deep water waves
;
; File name for sensors
SENSORFILE=ffg8                         Output file names with case suffix

; Electromagnetic frequency (GHz), Incidence angle
; (degrees), temperature (degrees centigrade) and
; salinity (ppt)
;
EF=1.25                                 L-band
INCANG=29.000                           In table
TEMP=15.000                             Default
SAL=35.000                              Default
;
; Number of rows and columns in sensor simulation,
;
NXCOLS=256                              Not used for sensor=stats
NYROWS=256                              Not used for sensor=stats
LCUT=1                                  Use this value for sensor=stats
FOCUS=1.000                             Not used for sensor=stats
;
; Origin of input and output grids (m) and
; angle of rotation of output grid (degrees)
;
XORGNI=0.000                            Defaults for hydro origin, offset from
innis origin
YORGNI=0.000                            Defaults for hydro origin, offset
XORGNO=0.000                            Do entire hydro grid
YORGNO=0.000                            Do entire hydro grid
ANGROT=0.000                            Rotation wrt hydro grid
;
; Additional SAR parameters, Polarization, azimuth
; resolution (m), platform velocity (m/s),
; range (m), sensor type, and sensor filename
;
POLAR=vv                                Always vv for this test
AZRES=2.16
VEL=200.000
RANGE=4200.000                          Not used for sensor=stats
SENSOR=psar                             This scales output to e.m. grid
XPIXEL=0.5
YPIXEL=10.
ISEED=1234567                           Not used for sensor=stats
```

FILTFAC=1.000Not used for sensor=stats
BAPT=0.000 Not used for NAPT=1
ZAPT=0.000 Not used for NAPT=1
NAPT=1 1 antenna
RHS=8 Quadratic with turbulence
IOSTYLE=nrl NRL output format
DualBragg=.False.
SaveComplex=.False. Don't save complex image
RSLWAVE Run RSLWAVE
iostyle=erim To put out data files with no header for SOS

ZSIM Create gridded RCS, MRV, and VRV
EXIT

RUN SOSNEW4

Enter sample spacings in range and azimuth(m):
2.16 8.64
Enter no. of columns and rows (power of two):
600 70
Enter platform velocity(m/s) and altitude(km):
128. 4.2
Enter incidence angle (+ for right-looking, - for left-looking):
+45. Right or Left
Enter radar wavelength(cm) and resolution(m):
23.5 2.16
Integration time = 0.09 sec
Azimuth bandwidth = 51.2 Hz
Enter magnitude of hydro. and tilt mtf:
1. 1.
Enter r.m.s. radial velocity(m/s) due to sub-resolution-scale waves:
.1
Enter output file name for Fourier coefficients:
sosfourier.dat
Randomize Fourier amplitudes as well as phases?
N
Enter seed for random number generator:
123456

APPENDIX C. FALSECOLOR 2-D RCS IMAGES OF CENTERLINE SHIPWAKES

The following 16 falsecolor images are referenced by Case number to the conditions in Tables 1 and 2. The colorbar for translating into relative RCS units is below the image. The centerline shipwake is expanded in the crosswake direction in order to make the details more visible (except for Cases 12, 15, and 16 which are at 1:1 scale).

In order to produce the RCS image including SAR modulation transfer effects due to the waves, the SOS program was run with the outputs of the ZSIM module in EOM. A typical SOS command file (including prompts) is shown below:

ONR
SSWD

EOM CENTERLINE WAKE SIMULATION

ERIM

92-20316.16

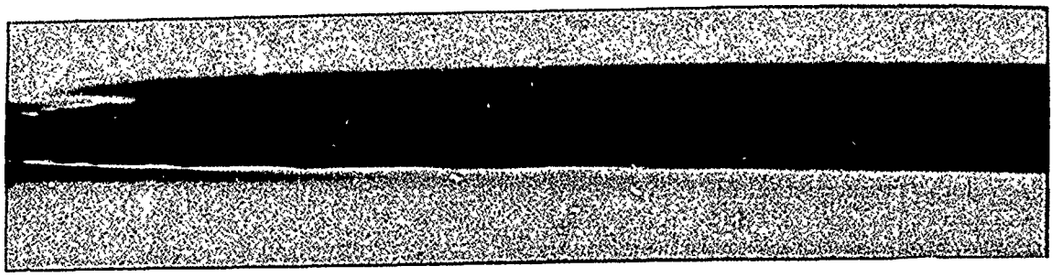

Ship Type: DDG	Band/Polarization: LVV
Ship Speed: 18 kn	Incidence Angle: 50°
Ship Heading: 55°	Image Size
Wind Speed: 22 kn	Range: 150 m
Wind Direction: 50°	Azimuth: 4750 m

Case 1

ONR
SSWD

EOM CENTERLINE WAKE SIMULATION

ERIM

92-20316.15

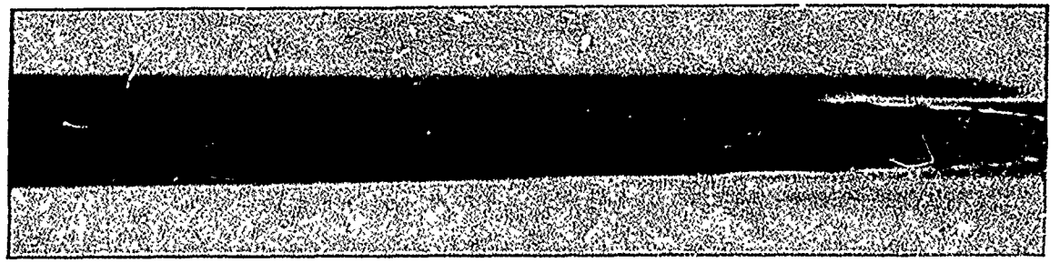

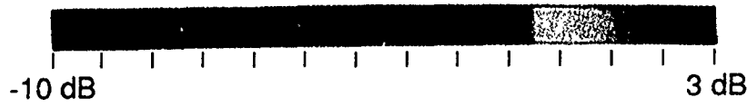

Ship Type: DDG	Band/Polarization: LVV
Ship Speed: 18 kn	Incidence Angle: 36°
Ship Heading: 55°	Image Size
Wind Speed: 22 kn	Range: 150 m
Wind Direction: 50°	Azimuth: 4750 m

Case 2

ONR
SSWD

EOM CENTERLINE WAKE SIMULATION

ERIM

92-20316.14

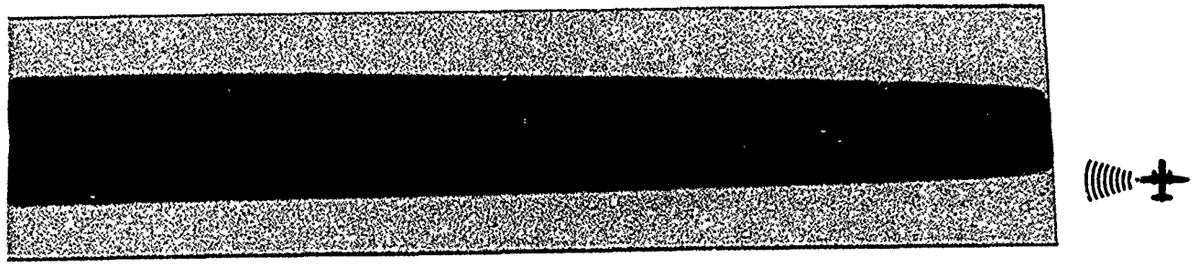

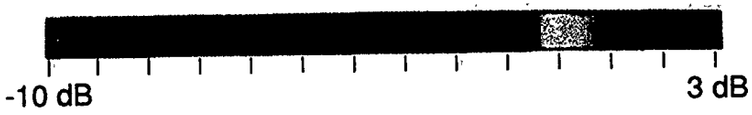

Ship Type: DDG	Band/Polarization: LVV
Ship Speed: 18 kn	Incidence Angle: 50°
Ship Heading: 210°	Image Size
Wind Speed: 7.5 kn	Range: 4900 m
Wind Direction: 295°	Azimuth: 150 m

Case 3

ONR
SSWD

EOM CENTERLINE WAKE SIMULATION

ERIM

92-20316.13

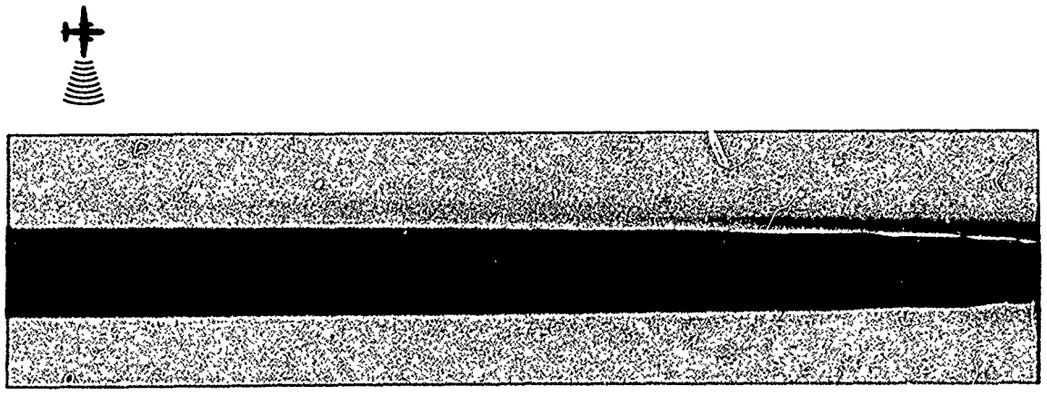

Ship Type: DDG	Band/Polarization: LVV
Ship Speed: 18 kn	Incidence Angle: 50°
Ship Heading: 210°	Image Size
Wind Speed: 9.5 kn	Range: 150 m
Wind Direction: 310°	Azimuth: 4750 m

Case 4

ONR
SSWD

EOM CENTERLINE WAKE SIMULATION

ERIM

92-20316.12

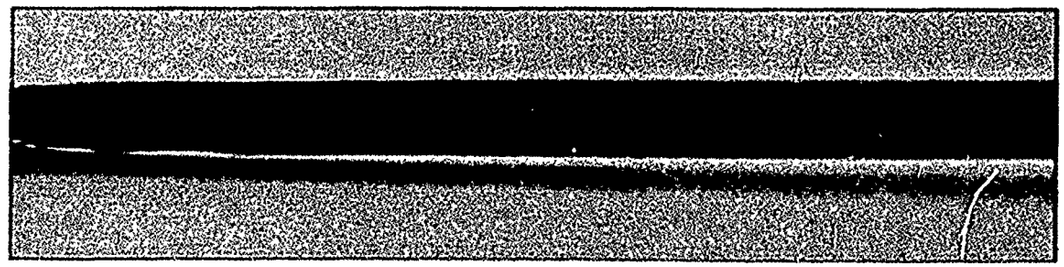

Ship Type: DDG	Band/Polarization: LVV
Ship Speed: 18 kn	Incidence Angle: 27°
Ship Heading: 210°	Image Size
Wind Speed: 9 kn	Range: 150 m
Wind Direction: 290°	Azimuth: 4750 m

Case 5

ONR
SSWD

EOM CENTERLINE WAKE SIMULATION

ERIM

92-20316.11

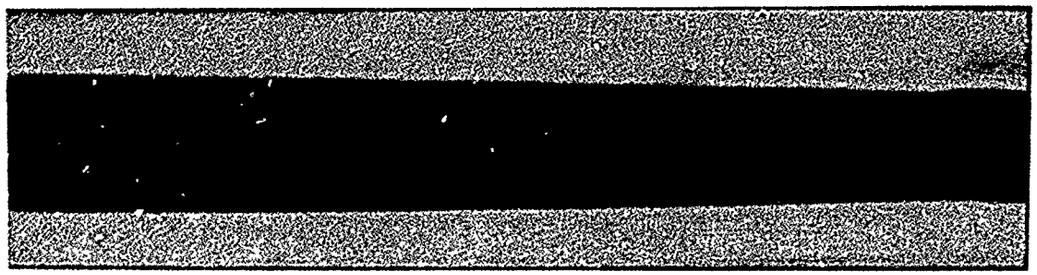

-10 dB 3 dB

Ship Type: DDG	Band/Polarization: LVV
Ship Speed: 18 kn	Incidence Angle: 55°
Ship Heading: 210°	Image Size
Wind Speed: 6.0 kn	Range: 4900 m
Wind Direction: 300°	Azimuth: 150 m

Case 6

ONR
SSWD

EOM CENTERLINE WAKE SIMULATION

ERIM

92-20316.10

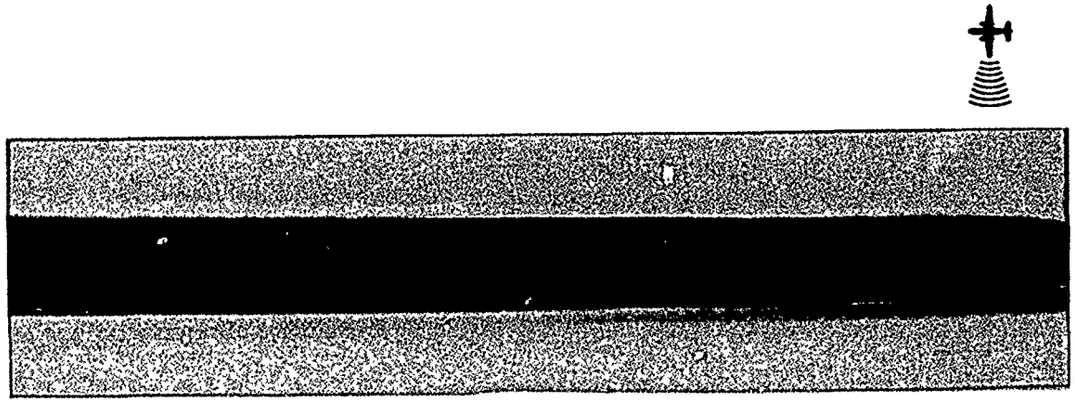

Ship Type: DDG	Band/Polarization: LVV
Ship Speed: 18 kn	Incidence Angle: 44°
Ship Heading: 205°	Image Size
Wind Speed: 22 kn	Range: 150 m
Wind Direction: 50°	Azimuth: 4750 m

Case 7

ONR
SSWD

EOM CENTERLINE WAKE SIMULATION

ERIM

92-20316.9

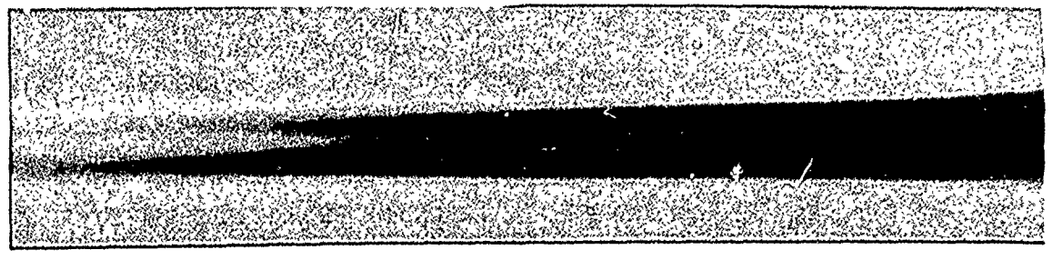

Ship Type: FFG	Band/Polarization: LVV
Ship Speed: 18 kn	Incidence Angle: 54°
Ship Heading: 210°	Image Size
Wind Speed: 18 kn	Range: 4900 m
Wind Direction: 0°	Azimuth: 150 m

Case 8

ONR
SSWD

EOM CENTERLINE WAKE SIMULATION

ERIM

92-20316.2

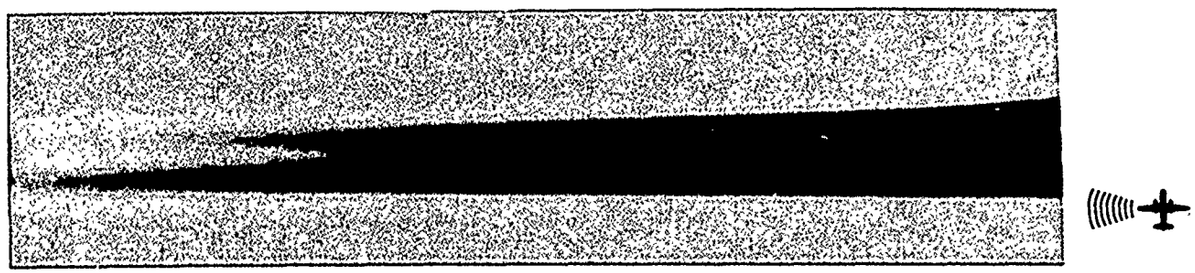

Ship Type: FFG	Band/Polarization: LVV
Ship Speed: 18 kn	Incidence Angle: 62°
Ship Heading: 210°	Image Size
Wind Speed: 18 kn	Range: 4900 m
Wind Direction: 5°	Azimuth: 150 m

Case 9

ONR
SSWD

EOM CENTERLINE WAKE SIMULATION

ERIM

92-20316.5

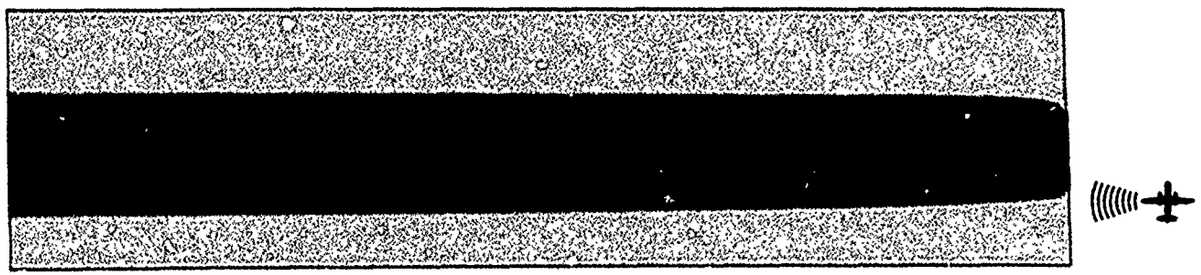

Ship Type: FF	Band/Polarization: LVV
Ship Speed: 18 kn	Incidence Angle: 46°
Ship Heading: 210°	Image Size
Wind Speed: 9 kn	Range: 4900 m
Wind Direction: 250°	Azimuth: 150 m

Case 10

ONR
SSWD

EOM CENTERLINE WAKE SIMULATION

ERIM

92-20316.7

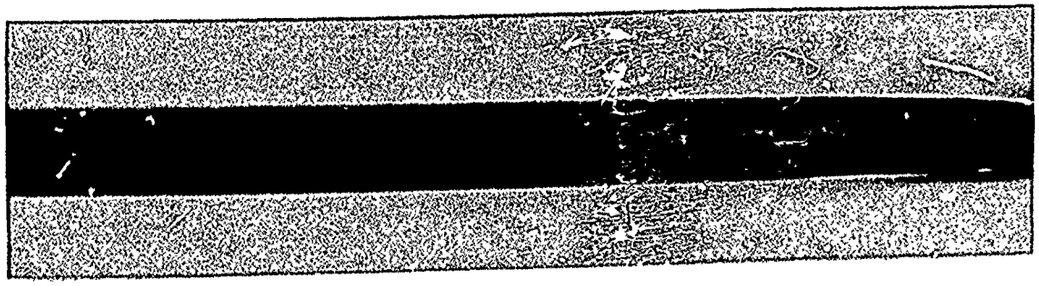

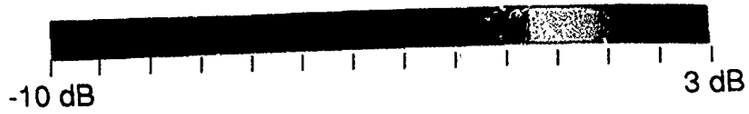

Ship Type: FF	Band/Polarization: LVV
Ship Speed: 18 kn	Incidence Angle: 49°
Ship Heading: 210°	Image Size
Wind Speed: 8 kn	Range: 150 m
Wind Direction: 277°	Azimuth: 4750 m

Case 11

ONR
SSWD

EOM CENTERLINE WAKE SIMULATION

ERIM

92-20316.8

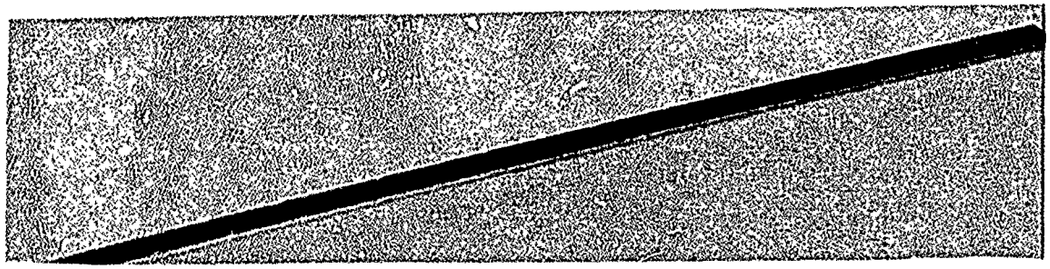

Ship Type: FF	Band/Polarization: LVV
Ship Speed: 18 kn	Incidence Angle: 23°
Ship Heading: 210°	Image Size
Wind Speed: 8.5 kn	Range: 600 m
Wind Direction: 270°	Azimuth: 2450 m

Case 12

ONR
SSWD

EOM CENTERLINE WAKE SIMULATION

ERIM

92-20316.4

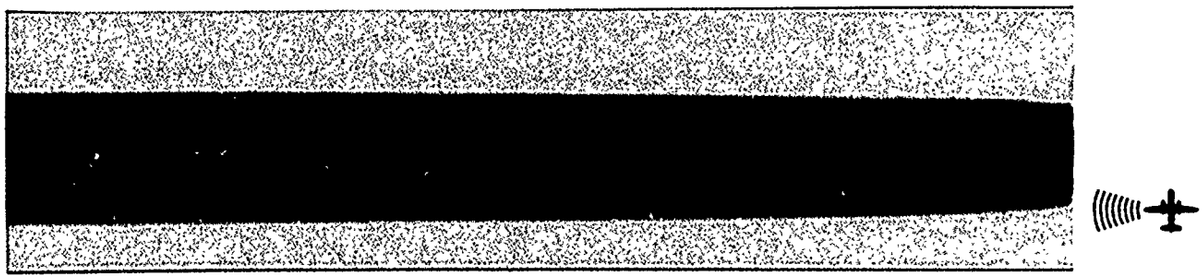

Ship Type: FF	Band/Polarization: LVV
Ship Speed: 18 kn	Incidence Angle: 64°
Ship Heading: 210°	Image Size
Wind Speed: 8 kn	Range: 4900 m
Wind Direction: 240°	Azimuth: 150 m

Case 13

ONR
SSWD

EOM CENTERLINE WAKE SIMULATION

ERIM

92-20316.3

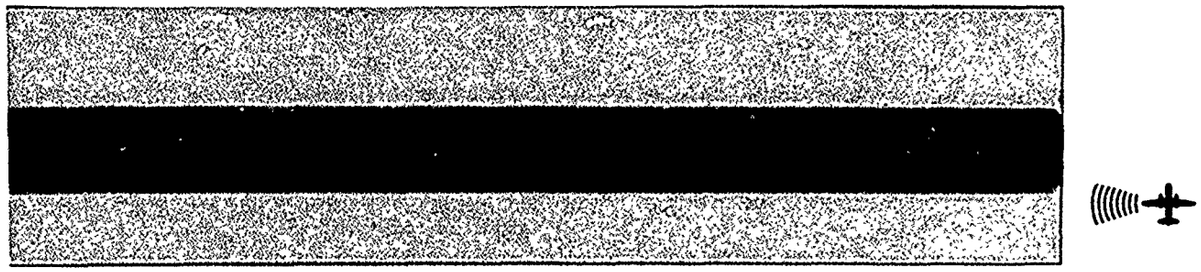

Ship Type: FFG	Band/Polarization: LVV
Ship Speed: 18 kn	Incidence Angle: 47°
Ship Heading: 210°	Image Size
Wind Speed: 8 kn	Range: 4900 m
Wind Direction: 240°	Azimuth: 150 m

Case 14

ONR
SSWD

EOM CENTERLINE WAKE SIMULATION

ERIM

92-20316.1

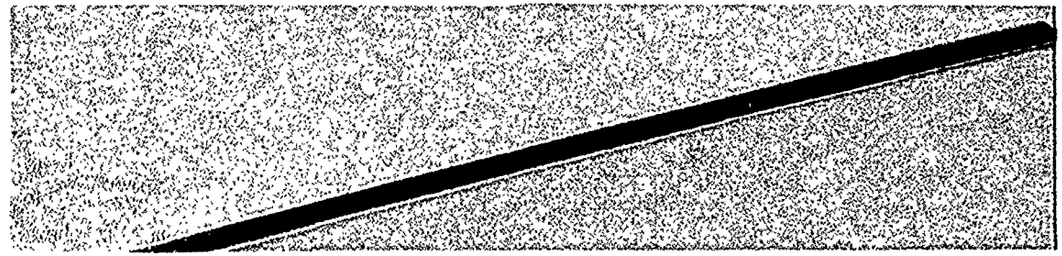

Ship Type: FF	Band/Polarization: LVV
Ship Speed: 18 kn	Incidence Angle: 21°
Ship Heading: 210°	Image Size
Wind Speed: 8 kn	Range: 600 m
Wind Direction: 250°	Azimuth: 2450 m

Case 15

ONR
SSWD

EOM CENTERLINE WAKE SIMULATION

ERIM

92-20316.6

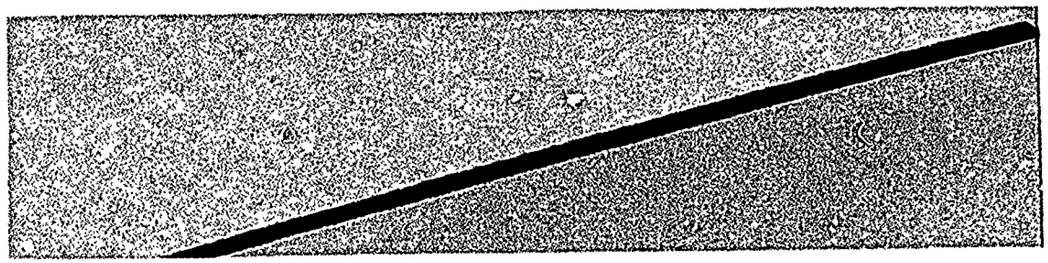

Ship Type: FFG	Band/Polarization: LVV
Ship Speed: 18 kn	Incidence Angle: 21°
Ship Heading: 210°	Image Size
Wind Speed: 8 kn	Range: 600 m
Wind Direction: 250°	Azimuth: 2450 m

Case 16